JOURNAL OF SOLID STATE CHEMISTRY 4, 400–409 (1972)

Neutron Diffraction and Other Studies of Magnetic Ordering in Phases Based on Cr_2O_3, V_2O_3 and Ti_2O_3

A. F. REID

C.S.I.R.O., Division of Mineral Chemistry, Box 124, Port Melbourne, Victoria, 3207, Australia

T. M. SABINE

A.A.E.C. Research Establishment, Lucas Heights, N.S.W., 2232, Australia

AND

D. A. WHEELER

Australian Institute of Nuclear Science and Engineering, Lucas Heights, N.S.W., 2232, Australia

Received August 23, 1971

Solid solutions in the Cr_2O_3–V_2O_3 and Cr_2O_3–Ti_2O_3 systems have been examined by neutron diffraction, X-ray diffraction, electron spin resonance and magnetic susceptibility methods. In $(Cr_xV_{1-x})_2O_3$ the low temperature monoclinic V_2O_3 phase was found to extend from $x = 0$ to $x = 0.5$. Long-range order in this phase disappears gradually as x increases. For $0.4 < x < 1.0$ two kinds of antiferromagnetic order were observed both based on the Cr_2O_3 magnetic structure. In $(Cr_xTi_{1-x})_2O_3$ only the Cr_2O_3-type antiferromagnetic structure was found with the Ti^{3+} ions acting as a simple diluent.

The electron spin resonance signal from Cr^{3+} in $(Cr_xV_{1-x})_2O_3$ is found to be quenched by dipolar interaction with V^{3+}; however, that for Ti^{3+} in $(Cr_xTi_{1-x})_2O_3$ is observable above and below the temperature for Cr^{3+} spin ordering.

The lattice parameters for the $(Cr_xV_{1-x})_2O_3$ system show a sharp discontinuity in the region $0 < x < 0.02$. From the data outside this region an ionic radius for paramagnetic V^{3+} of 0.645 Å is derived.

It is found that, for many corundum-structure magnetic systems, ordering is independent of the spin state of the diluent atoms.

1. Introduction

The transition-metal sesquioxides Cr_2O_3 and V_2O_3 have the corundum structure at high temperature and form a continuous series of solid solutions. Cr_2O_3 is an antiferromagnetic (AFM) insulator with a Néel temperature of 306 ± 2°K (*1*). It has the corundum structure at all temperatures. V_2O_3 is a metallic conductor at room temperature and at 150–160°K transforms to a monoclinic phase which is semiconducting (*2*).

Measurement of various physical properties (*3*) had indicated that the low-temperature phase was antiferromagnetic but the results of neutron diffraction experiments had not confirmed this. Paoletti and Pickart (*4*) found an additional low-angle peak at low temperature and interpreted it as due to a structural change. Kendrick, Arrott and Werner (*5*) had looked for antiferromagnetism of the Fe_2O_3 type without success but their experiments did not rule out antiferromagnetism of the Cr_2O_3 type.

During our work, which was commenced to determine the magnetic phase diagram for the Cr_2O_3–V_2O_3 system, Moon (*6*) carried out a definitive experiment using the new technique of polarization analysis (*7*) and showed that the low-temperature phase of V_2O_3 was antiferromagnetic. During this period also, Menth and Remeika (*8*) studied the magnetic susceptibility of the V_2O_3–Cr_2O_3 system, particularly at the V_2O_3-rich end, and derived a phase diagram based on observed maxima and minima in magnetic susceptibility vs temperature.

Our neutron-diffraction results show a magnetic and structural phase diagram which agrees in part with that of Menth and Remeika, but shows a

© 1972 by Academic Press, Inc.

number of features which the susceptibility studies did not detect. Our other observations have, in addition, shown that for most corundum solid solutions, the spin-order regimes of one kind of ion are independent of those of a second kind. Various other properties of these compounds are also discussed.

2. Experimental

2.1. Preparations

Specimens of $CrVO_3$ were prepared by hydrogen reduction of $CrVO_4$, a compound in which Cr and V are completely ordered (*9*) and which should therefore provide the best possible mixing of Cr^{3+} and V^{3+} in the corundum structure resulting from reduction. $CrVO_4$ was prepared by heating ammonium vanadate and finely divided Cr_2O_3 first at 600°C and then at 850°C for several periods of 20 hr with intermittent regrinding. Despite these precautions, a small amount of free Cr_2O_3 was always present (*10*), and remained so after reduction at 600°C to 1000°C. However, after regrinding and reheating in hydrogen at 1200°C the $CrVO_3$ was homogeneous, and had essentially the same lattice parameter when reheated in hydrogen up to 1450°C. ($CrVO_4$ produced by oxidation of this product contained no free Cr_2O_3.) Specimens of $(Cr_xV_{1-x})_2O_3$ were prepared by mixing and grinding either additional Cr_2O_3 or V_2O_5 with $CrVO_4$, reducing these mixtures at 900°–1000°C and then heating the reground and pelleted mixtures at 1200°–1450°C in a slow stream of purified hydrogen. Microprobe traces showed a constant Cr:V ratio across a large number of grains. For compositions close to V_2O_3, a temperature not higher than 1150°–1200°C was necessary, otherwise the lines of VO were discernible in the X-ray powder patterns.

The conclusions drawn by Rubinstein (*11*) in his NMR study of Cr-doped V_2O_3, particularly with respect to the inhomogeneous nature of the metallic transition, may be due in part to the temperature of preparation of his samples, 1350°C.

$(Cr_{1-x}Ti_x)_2O_3$ specimens were prepared by heating an intimately ground, pelleted mixture of Cr_2O_3 and anatase-form TiO_2 in hydrogen at 1300°–1500°C for 15 to 20 hr. $CrTiO_3$ thus produced was particularly well crystallized, with a grain size of the order of 0.2 mm, and showed remarkable resistance to oxidation at elevated temperatures. The $CrAlO_3$ sample, used by Sabine and Vance in their neutron diffraction study (*12*), was prepared from coprecipitated hydroxides, with a final firing temperature of 1400°C.

2.2. X-ray and Neutron Diffraction

X-Ray lattice parameters were refined by least squares using powder data obtained with a Guinier focusing camera using monochromatized Cu$K\alpha$ radiation, $\lambda = 1.54051$ Å, and with KCl, $a_0 = 6.2931$ Å, as an internal standard. X-Ray reflection intensities were measured from slow scan patterns obtained with a Philips diffractometer. Admixture of Cr_2O_3 with $CrVO_3$ showed that less than 1% of free Cr_2O_3 could be detected from the powder patterns.

Neutron diffraction patterns were taken at 4.2°K, 77°K and room temperature on a conventional double-axis neutron powder diffractometer installed on the HIFAR reactor. This diffractometer is equipped with a variable temperature cryostat providing continuous variation of temperature between 4.2°K and 400°K. Phase-transformation temperatures were found by measurements of the variation of intensity of selected neutron reflections with temperature.

2.3. Electron Spin Resonance and Magnetic Susceptibility

ESR spectra were obtained for temperatures from 77°K to 400°K using a conventional 9 GHz spectrometer. Magnetic susceptibilities were determined on powdered samples by the Gouy method. No ferromagnetic impurities could be detected.

3. Results

3.1. Crystal Structures

3.1.1. Cr_2O_3–V_2O_3 System. At room temperature the Cr_2O_3–V_2O_3 solid solution series, including V_2O_3, are isostructural with α-Al_2O_3, space group $R\bar{3}c$ (No. 167). In the hexagonal setting, metal atoms occupy positions 12(*c*) and oxygen atoms 18(*e*). In the idealized structure, oxygen atoms are hexagonally close packed, with positional parameters 1/3, 0, 1/4. The octahedral sites thus created are only two-thirds occupied, with the metal atoms having idealized parameters 0, 0, 1/3. In the real structures the distortion from hexagonal close packing gives the *x*-coordinate for oxygen a value near to 0.31 and the *z*-coordinate a value near 0.35 (*13*). Single-crystal determinations have been made for a number of corundums, including Cr_2O_3 (*14*), V_2O_3 (*15*) and $(Cr_{0.038}V_{0.962})_2O_3$ (*15*).

The lattice parameters in the Cr_2O_3–V_2O_3 system, Table I, Figs. 1 and 2, show a very large discontinuity between $(Cr_{0.02}V_{0.98})_2O_3$ and V_2O_3. This has now been amply documented (*17*) as a concomitant of the metal to insulator, or more

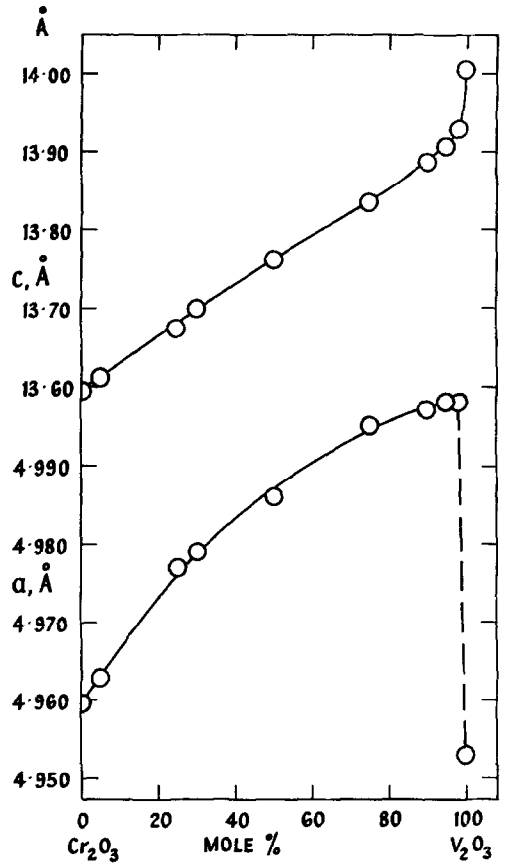

FIG. 1. Lattice parameters of $(Cr_xV_{1-x})_2O_3$ compositions.

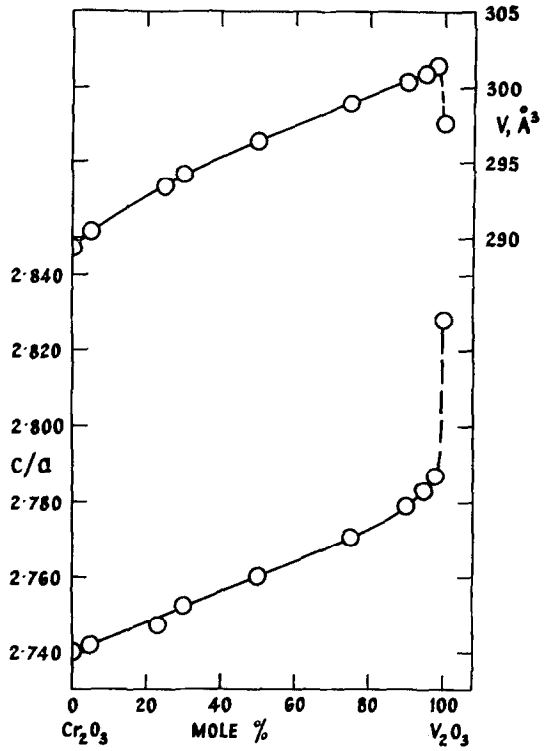

FIG. 2. Molar volumes and c/a ratios for $(Cr_xV_{1-x})_2O_3$ compositions.

properly, metal to semiconductor, transition which is induced in V_2O_3 by addition of ~1% of Cr_2O_3 to the structure. Dernier (*14*) has shown from single-crystal structure refinements that this transformation, as well as being accompanied by a volume change of 1.3%, Table I, is accompanied by a marked change in V–V separation similar to that which occurs when V_2O_3 is cooled below 150°K and the metallic corundum structure converts to one which is monoclinic and semiconducting. For our ceramic samples, interpolated lattice parameters for $(Cr_{0.038}V_{0.962})_2O_3$ and the values for V_2O_3 agree very closely with those of Dernier for flux-grown material (*15*). Extrapolation of the continuous portion of the unit cell volume curve to $x = 1.00$ gives a volume of 301.5 Å^3, which is the volume that corundum type V_2O_3 would have without the strong V^{3+}–V^{3+} interaction, and which characterizes the V^{3+} ion in semiconducting or insulating corundum lattices. This volume is almost identical with that of Fe_2O_3, 301.88 Å^3 and gives V^{3+} ion an ionic radius of 0.645 Å, on the basis that molar volume is a direct function of ionic radius (*13, 19*).

TABLE I

LATTICE PARAMETERS $(Cr_xV_{1-x})_2O_3$

x	a (±0.001 Å)	c (±0.003 Å)	c/a	V (±0.1 Å^3)
1[a]	4.959	13.595	2.740	289.2
0.95	4.963	13.610	2.742	290.3
0.75	4.977	13.674	2.747	293.3
0.70	4.979	13.700	2.752	294.1
0.50	4.986	13.762	2.760	296.3
0.25	4.995	13.835	2.770	298.9
0.10	4.997	13.886	2.779	300.3
0.05	4.998	13.909	2.783	300.9
0.02	4.998	13.930	2.787	301.4
0[b]	4.953	14.005	2.828	297.5

[a] Made from analytical-grade ammonium dichromate with a final heat at 1200°C. Newnham and de Haan (*14*) give $a = 4.958$, $c = 13.587$. NBS values (*16*) are $a = 4.954$, $c = 13.584$.

[b] Made by H_2 reduction of analytical-grade ammonium vanadate at 1000°C. Newnham and de Haan (*14*) give $a = 4.952$, $c = 14.002$ for flame fusion material, and Dernier (*15*) $a = 4.9515$, $c = 14.003$ for flux-grown crystals.

TABLE II

ATOMIC COORDINATES FOR Cr_2O_3–V_2O_3 COMPOSITIONS

	Oxygen coord. x	(Cr, V) Coord. z	Method	Reference
Cr_2O_3	0.306 (4)	0.3475 (3)	Single crystal	(*14*)
$CrVO_3$	0.304 (2)	0.342 (7)	Neutron[a]	This work
$CrVO_3$	0.307 (8)	0.346 (2)	X-ray[a]	This work
$(Cr_{0.05}V_{0.95})_2O_3$	0.306 (8)	0.346 (2)	X-ray[a]	This work
$(Cr_{0.038}V_{0.962})_2O_3$	0.30745 (17)	0.34869 (2)	Single crystal	(*15*)
V_2O_3	0.31164 (14)	0.3463 (2)	Single crystal	(*15*)

[a] Powder diffraction data.

From X-ray diffractometer intensity data taken for $CrVO_3$ (25 reflections) and $(Cr_{0.05}V_{0.95})_2O_3$ (26 reflections) and from neutron data for $CrVO_3$ (22 reflections) we have derived atomic coordinates by least-squares refinement of the resulting structure factors. These coordinates are shown in Table II, together with single-crystal values for Cr_2O_3 $(Cr_{0.038}V_{0.962})_2O_3$ and V_2O_3. It is seen that within experimental error, the fractional coordinates remain constant across the solid-solution range, changing only for the end-member V_2O_3.

The volume increase obtained in V_2O_3, when Cr_2O_3 is added to the lattice, is also observed with additions of Fe_2O_3 and Al_2O_3 (*17*), although lattice parameters have not been reported. The lower molar volume for the metallic phase implies that it can be produced at higher concentrations of a second component by the application of pressure, and indeed $(Cr_xV_{1-x})_2O_3$ compositions which are insulating (semiconducting) at zero pressure can be made metallic at elevated pressures (*17*, *19*). In the Al_2O_3–V_2O_3 system the defect spinel $AlVO_3$ (*20*) when subjected to very high pressure (100 kbar at 900°C) disproportionates to two corundum phases, one essentially pure Al_2O_3, the other an $(Al, V)_2O_3$ composition with zero-pressure lattice parameters $a = 4.982$ Å, $c = 13.86$ Å. Assuming a lattice-parameter curve similar in shape to that for Cr_2O_3–V_2O_3, this approximates to a composition $(Al_{0.1}V_{0.9})_2O_3$. It would appear that exsolution of Al_2O_3 from $AlVO_3$ just allows metallic phase formation for this composition at 100 kbar, 900°C, with a consequent reduction in phase volume. The Al_2O_3–V_2O_3 corundum shows a central immiscibility region (*21*) which should have been narrowed by increasing pressure but was instead widened, and the formation of a metallic phase of reduced volume would provide an explanation for this behaviour.

3.1.2. Monoclinic Low-Temperature Phase in the $(Cr_xV_{1-x})_2O_3$ System. The crystal structure of monoclinic V_2O_3 has been determined by Dernier and Marezio (*22*). It involves a distortion from the hexagonal cell in which the vanadium–vanadium distance across the shared octahedral face increases and at the same time the vanadium atoms move towards adjacent octahedral voids so that the vanadium–vanadium edge-shared distance is also increased. Although the change in symmetry and the distortion of structure in going from hexagonal to AFM monoclinic type is particularly pronounced, a comparable change of symmetry from cubic to rhombohedral, also ascribable to magnetostrictive forces, is observed when NiO and MnO become antiferromagnetic (*3*).

Resistivity and X-ray diffraction observations (*15*) show that for V_2O_3 and $(Cr_{0.01}V_{0.99})_2O_3$ the change from semiconducting to metallic behaviour is coincident with the phase change from monoclinic to corundum form, and the neutron diffraction studies by Moon (*6*) show that this phase change is also coincident with the disappearance of antiferromagnetism. A pronounced specific heat effect is also observed at the transition (*23*, *24*).

In our neutron diffraction observations, the crystallographic identification of the monoclinic phase was based on the (001) and (201) reflections, as well as the (011), (200) doublet, Fig. 3. As x increases, this doublet coalesces at the position of the (012) reflection of the hexagonal phase, but contains no magnetic contribution for $x < 0.3$.

Our results show that at appropriate temperatures the monoclinic structure extends from $x = 0$ to $x = 0.5$. For this composition region Menth and Remeika (*8*) observed a series of rather broad magnetic susceptibility maxima at temperatures which, although somewhat above the monoclinic-

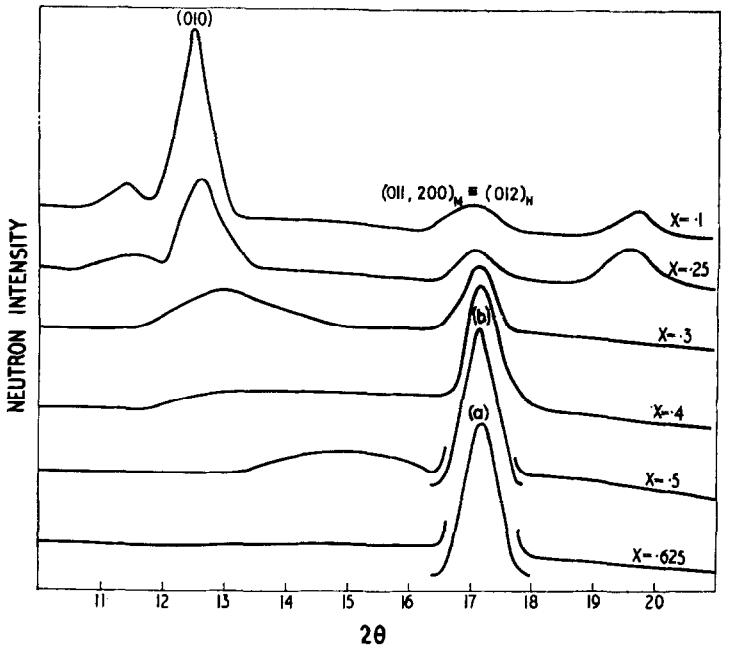

FIG. 3. Neutron powder diffraction patterns of $Cr_x(V_{1-x})_2O_3$ at 4.2°K, $\lambda = 1.07$ Å. For $x \leqslant 0.3$ the structure is monoclinic, and for $x > 0.3$, hexagonal. Peak (b), $x = 0.5$, is shown reduced in height by a factor of 5, and peak (a), $x = 0.625$, is reduced by 10. Vanadium has negligible coherent scattering length for neutrons, and the Bragg peak $(011, 200)_{\text{Monoclinic}}$ is mainly due to oxygen scattering. As the Cr content increases, a small increase in nuclear scattering is noted. Above $x = 0.3$, the peak is $(012)_{\text{Hexagonal}}$ and has a magnetic as well as a nuclear contribution.

hexagonal phase boundary determined in the present work, can probably be associated with the transition.

3.1.3. Cr_2O_3–Ti_2O_3 System. As the Néel temperature behaviour of the Cr_2O_3–V_2O_3 system for $x > 0.3$ was very similar to that found for Cr_2O_3–Al_2O_3 (*12*), we decided also to examine a system containing an end number which was paramagnetic but did not itself show antiferromagnetism (*7*). Between Cr_2O_3 and at least $CrTiO_3$, we found Ti_2O_3 to form a homogeneous corundum-type solid solution with Cr_2O_3. The *c* axis lattice parameters showed considerable scatter, also a feature of Ti_2O_3 preparations (*13*) and attributable to structural sensitivity to small departures from stoichiometry. However, the *a* axis values changed smoothly with composition. For $CrTiO_3$, which appeared to be a particularly strongly forming composition, $a_0 = 5.050 \pm 0.005$, $c_0 = 13.630 \pm 0.005$ for preparations at both 1300°C and 1450°C. Below the Néel temperature, $CrTiO_3$ retained the corundum structure.

3.2. Electron Spin Resonance

For Cr_2O_3 or Cr_2O_3 containing 10% of Al_2O_3 in solid solution, an intense Cr^{3+} spin resonance signal with $g = 2.00$ and linewidth ~500 G is obtained at temperatures above the Néel point (*25*, *26*). As the spin resonance signal of V^{3+} is rarely observed above 4°K due to its very short relaxation time, it was thought possible to observe similar spectra in $(Cr_xV_{1-x})_2O_3$ compositions above their Néel temperatures. A strong signal was indeed obtained for $x = 0.95$, but with a linewidth of 3400 G. At $x = 0.90$ the signal was even broader and very much weaker, and by $x < 0.80$ was absent, even when the sample temperature was 400°K. For $CrVO_3$ at 300°K to 400°K the intensity of the very weak residual signal obtained at high gain was compared with that of Cr_2O_3 mechanically diluted with Al_2O_3, and found to correspond to less than 0.02% of free Cr_2O_3, supposing this to be the source of the signal. Since we shall show that V^{3+} spins do not order within the Cr^{3+} spin system, we conclude that the Cr^{3+} spin system has its relaxation time greatly reduced by dipole–dipole interaction associated with the very rapid reversals of spin alignment of the $3d^2$ electrons of V^{3+}.

For both $(Cr_{0.9}Ti_{0.1})_2O_3$ and $CrTiO_3$, there was a very intense ESR signal centred at $g = 2.00$ and of linewidth ≈ 1600 G, very much greater than in $(Cr_{0.9}Al_{0.1})_2O_3$, 500 G, or $CrAlO_3$, 250 G (*26*). This signal was unaltered below the Néel points for these compositions and was evidently primarily

due to Ti^{3+}, together with a smaller Cr^{3+} contribution above the Néel points.

3.3. Magnetic Susceptibilities

The magnetic susceptibilities of $CrVO_3$, $CrTiO_3$ and $CrAlO_3$ are shown in Fig. 4, together with those for several other AFM V^{3+} compounds. The $CrVO_3$ values are consistent with those of Menth and Remeika (*8*) for $(Cr_{0.3}V_{0.7})_2O_4$ and $(Cr_{0.6}V_{0.4})_2O_3$, and show a very broad maximum in the region of the Néel point. For both $CrTiO_3$ and $CrAlO_3$ the susceptibilities did not show an inflection near the Néel point but instead for this temperature range increased steadily with decrease in temperature. A similar behaviour has been observed for compositions in the Cr_2O_3–Fe_2O_3 system (*27*) and ascribed to fluctuations in ordering which persist until lower temperatures are reached.

The differences between the $CrTiO_3$ and $CrAlO_3$ susceptibilities are reasonably close to the gram-atom values for spin-only Ti^{3+}, i.e., 2.52×10^{-3} at 100°K and 1.24 at 200°K, similar to the values observed for $ScTiO_{3.053}$ (*28*), 2.50×10^{-3} and 1.50×10^{-3}, respectively. These results, together with the ESR observations, show that the Ti^{3+} spin system is not magnetically coupled to that of Cr^{3+}, and also that the spin cancellation observed in Ti_2O_3 itself due to *c*-axis spin pairing (*29*) has been removed. The associated metallic conductivity is also absent, and a sintered compact of $CrTiO_3$ had a resistivity of approximately 10^6 ohm-cm at room temperature.

The $CrVO_3$ results are indicative of a more complex situation than that in $CrAlO_3$ or $CrTiO_3$. Below 300°K the susceptibilities of $CrVO_3$ are lower than those for $CrTiO_3$, and below 200°K, lower than for $CrAlO_3$, continuing to decrease with decreasing temperature. The V^{3+} contribution to bulk susceptibility is thus very low, which indicates that strong short range V^{3+}–V^{3+} exchange coupling is operating in addition to Cr^{3+}–Cr^{3+} exchange coupling. This is consistent with the observation made below that for $CrVO_3$ there is a short temperature interval near 135°K where the monoclinic V_2O_3 structure type exists.

However, similar low V^{3+} contributions were observed for $(Cr_{0.6}V_{0.4})_2O_3$ (*8*) for which a monoclinic structure does not exist, and short-range V^{3+} coupling is apparently operating at this concentration also. It is noteworthy that the magnetic susceptibility of $(Cr_{0.04}V_{0.96})_2O_3$ is only slightly greater than the very low values shown by V_2O_3 itself, and shows the same discontinuity at the monoclinic → corundum phase transition boundary. Metallic conductivity in V_2O_3 is thus a property operating independently of the strong magnetic exchange coupling occurring both above and below the Néel point, and the presence of a few percent of Cr^{3+}, while disrupting the conduction band-structure, does not particularly affect the magnetic exchange coupling.

By contrast with the low susceptibility values found for V^{3+} in $CrVO_3$ and the AFM oxide compounds MgV_2O_4 (*30*, *31*), CaV_2O_4 (*30*, *32*) and $AlVO_3$ (*20*), Fig. 4, $ScVO_3$ of C-rare earth type shows a value of 2.93 μ_B for V^{3+}, very close to the "spin-only" value of 2.83 μ_B, and exhibits simple Curie–Weiss behaviour (*28*). These differences in

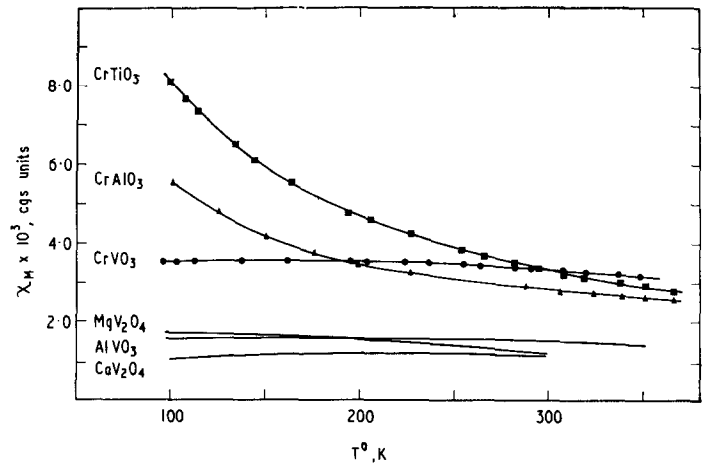

FIG. 4. Magnetic susceptibility as a function of temperature for $CrVO_3$, $CrTiO_3$ and $CrAlO_3$, together with the values for V^{3+} compounds $AlVO_3$ (*20*), MgV_2O_4 (*28*), and CaV_2O_4 (*28*). Gram-molar values, except for MgV_2O_4 and CaV_2O_4, for which the values per gram-ion of V^{3+} are given.

behaviour appear to be attributable to differences in V–V separations and possibly to differences in the regularity of repetition of edge or face sharing in the various structures. In $ScVO_3$, assuming Sc_2O_3 atomic coordinates (*33*) the closest V–V separation is 3.163 Å, across an octahedral edge, and metal atom sites connect in an irregular manner. In CaV_2O_4 (*32*) the V^{3+} ions occupy pairs of edge-shared octahedra repeating in infinite chains by additional edge sharing, with each V^{3+} having four near-neighbour V^{3+} atoms, two at 3.01 Å and two at 3.06 Å. In the spinel MgV_2O_4 the edge-shared V–V separations are 2.967 Å, and in the defect spinel $AlVO_3$, 2.978 Å. In $(Cr_xV_{1-x})_2O_3$ individual V–V octahedral face-shared separations are presumably less than or equal to those in the composition having $x = 0.038$, i.e., 2.746 Å (*14*).

It thus appears that in oxide compounds of V^{3+} which provide regular V–V separations of somewhat less than 3.1 Å, exchange coupling of V^{3+}–V^{3+} spins leads to a considerable lowering of effective spin even in paramagnetic situations and even when V^{3+} is occupying only a fraction of the available sites.

3.4. Magnetic Ordering in $(Cr_xV_{1-x})_2O_3$ and $CrTiO_3$

For low-temperature V_2O_3 Moon (*6*) found ferromagnetic coupling within (010) layers of the monoclinic body-centred unit cell (*22*) and antiferromagnetic coupling between layers. Monoclinic (010) corresponds to (110) hexagonal planes, and the zero-temperature atomic moment of 1.2 μ_B per V atom lies at approximately 71° to the hexagonal c axis. The moment is close to 1.06 μ_B observed by Hastings et al. for V^{3+} in antiferromagnetic CaV_2O_4 (*32*), and is to be compared with an ordered "spin-only" atomic moment of 2 μ_B[1]. Our experimental results for $x = 0.1$, 0.25, Fig. 3, showed a magnetic structure identical with that obtained by Moon for V_2O_3. The shift of $(001)_M$ and $(010)_M$ reflections to higher 2θ and the $(201)_M$ to lower 2θ are consistent with a lessening of the distortion involved in forming the monoclinic phase. However, for values of x between 0.3 and 0.5 the magnetic $(010)_M$ reflection becomes diffuse and its movement, Fig. 3, is much greater than that required to recover the hexagonal cell. A complex form of magnetic short-range order evidently occurs during the change from the V_2O_3 to Cr_2O_3 type AFM order. For $x < 0.3$ the intensities of the monoclinic reflections (011), (200) corresponding to the hexagonal (012) reflection used to determine Cr^{3+} antiferromagnetism were constant from 4°K to the transition temperature, indicating that there was no coherent ordering of the Cr_2O_3 type.

In antiferromagnetic Cr_2O_3, which has the corundum crystal structure both above and below the Néel point, the moments are oppositely directed in the pairs of Cr^{3+} atoms which share octahedral faces. The ordering of these pairs results in ferromagnetically aligned rows of Cr^{3+} atoms in the basal plane (*3*) with AFM coupling between adjacent planes. Magnetic susceptibility measurements on single-crystal Cr_2O_3 were used to demonstrate that the spins were antiferromagnetically aligned along the hexagonal c axis (*25*) and Corliss et al. (*34*) confirmed the spin direction by neutron diffraction and showed that the resultant zero-temperature atomic moment on the chromium atoms was $2.76 \pm 0.03\ \mu_B$.

As V_2O_3 is introduced into the Cr_2O_3 lattice the Néel temperature drops, following the same composition-temperature dependence as in the Cr_2O_3–Al_2O_3 system (*12*), including falling to zero temperature at $x = 0.30$. This behaviour indicates that V^{3+} spins are not directly affecting the degree of Cr^{3+} magnetic ordering. In order to examine a further case in which the diluent ion was paramagnetic but for which the end-member oxide (*7*) did not show spin ordering, the system Cr_2O_3–Ti_2O_3 was examined. For the composition $CrTiO_3$, a Néel temperature of 135 ± 3°K was found, almost identical with that for $CrVO_3$ and $CrAlO_3$, and arising from the same Cr_2O_3-type ordering.

3.5. Phase Diagram of $(Cr_xV_{1-x})_2O_3$

The variation with temperature of the intensities of the neutron diffraction reflections $(010)_M$ or $(012)_H$, Fig. 5, were used to define the magnetic phase boundaries shown in Fig. 6. No distinction was made between the sharp and diffuse $(010)_M$ reflections. For $0 < x < 0.4$ there is a low-temperature AFM monoclinic phase and a high-temperature paramagnetic corundum phase. The monoclinic transition temperature decreases linearly as x increases, and the transition becomes less sharp. Extrapolation of our values back to V_2O_3 gives a value of 168°K, close to that observed by Moon (*6*) for the monoclinic to hexagonal transition for pure V_2O_3 in the direction of increasing temperature.

[1] Use of $2S$, where S is the spin quantum number of the atom, for the "spin-only" value of μ_B, rather than the more usual $2\sqrt{[S(S+1)]}$, arises from the use of relative intensities of nuclear and magnetic neutron Bragg peaks to determine μ_B. The fraction of the total neutron scattering that can appear as coherent scattering, and thus able to give rise to Bragg reflections is $S/(S+1)$ of the scattering to be expected from a free ion of equal spin (*32*).

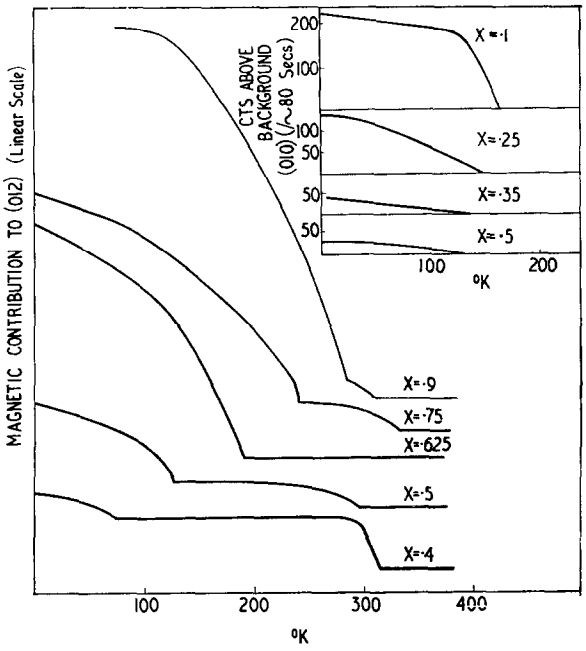

FIG. 5. Variation in neutron diffraction intensity with temperature for $(012)_{\text{Hexagonal}}$ and $(010)_{\text{Monoclinic}}$ reflections for the hexagonal and monoclinic regions of the Cr_2O_3–V_2O_3 system.

At $0.4 < x \leqslant 0.5$ there is a low-temperature Cr_2O_3-type hexagonal phase followed by magnetic short-range order in the monoclinic region above the hexagonal phase boundary. Above the temperature-composition line defining the monoclinic phase the crystal structure is again hexagonal. For $x > 0.3$, the low-temperature corundum-type phase has the same spin ordering as in AFM Cr_2O_3. From $x = 0.4$ to 0.9 however, a second step was observed in the intensity of the hexagonal (012) reflection, Fig. 5, corresponding to an upper magnetic transition at a temperature near 300°K, Fig. 6. The accuracy of the powder data does not allow the difference in magnetic structure between the low-temperature AFM corundum phase and the newly observed intermediate-temperature AFM phase to be deduced, but the changes in (012) intensity are far beyond experimental error.

Also shown in the phase diagram is the metallic region which, above 168°K, extends from V_2O_3 to $(Cr_xV_{1-x})_2O_3$ with $x \leqslant 0.009$ (*15*). This region is defined by the change from monoclinic, AFM V_2O_3 to metallic corundum type as a function of temperature increase, and by the abrupt change in c/a ratio (Fig. 2) and atomic coordinates (*15*) as the Cr composition increases. The metallic phase is thus bounded crystallographically as well as by extreme changes in electronic conductivity.

4. Discussion

4.1. Phase diagram

The phase diagram shown in Fig. 6 is broadly similar to that found by Menth and Remeika (*8*), but the use of neutron diffraction has enabled the

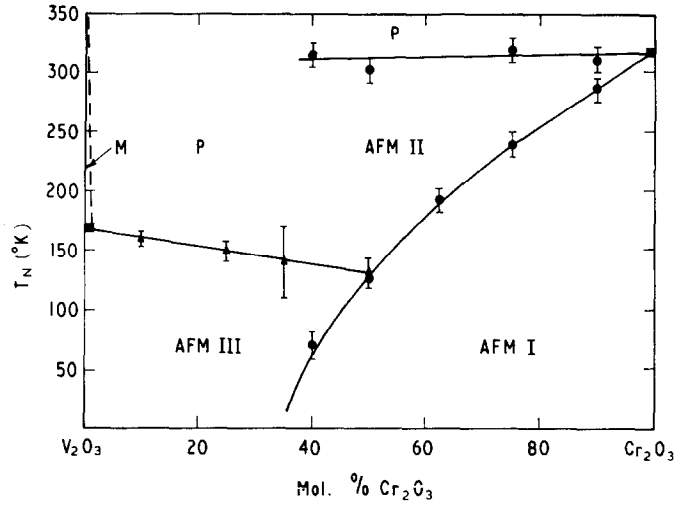

FIG. 6. Phase diagram for the system $(Cr_xV_{1-x})_2O_3$ defined by magnetic and crystallographic boundaries. Full lines determined by neutron diffraction, dashed line shows the metal-insulator boundary, which is also defined by a crystallographic discontinuity.

P: paramagnetic; AFM I: Cr_2O_3-type magnetic order, corundum lattice; AFM II: new and as yet unknown type of magnetic order, corundum lattice; AFM III; Monoclinic V_2O_3 type; M: metallic conduction, corundum lattice.

transition temperatures to be defined much more precisely. It has also confirmed the extension of the V_2O_3-type hexagonal-monoclinic transformation up to $x = 0.5$, and has disclosed the existence of an upper transition in the chromia-rich corundum region.

In his study of V_2O_3 spin ordering, Moon (*6*) observed an abrupt disappearance of the $(010)_M$ magnetic peak above 170°K, and the Brillouin curve normally characterizing a phase transition was sharply truncated. By extrapolation he found a Néel point of 283°K. However in our experiments on the semiconducting compositions $(Cr_xV_{1-x})_2O_3$, $x > 0.05$, curves which did not justify extrapolation were obtained, inset Fig. 5, and our transition temperatures extrapolated to $x = 0$ gave a value essentially identical with Moon's. Moon observed a 13°K hysteresis in AFM transition temperature on cooling from hexagonal to monoclinic form, and similar 12°K hysteresis is observed in the V_2O_3 resistance curves (*3*, *16*, *35*). Outside the metallic region, we observed little or no hysteresis, and McWhan and Remeika (*17*) also found it greatly diminished in single-crystal resistivity curves as Cr^{3+} content increased. The hysteresis also appears to be associated with metallic conductivity.

The nature of the upper corundum-based transition in $(Cr_xV_{1-x})_2O_3$ for $0.4 < x < 0.9$ is as yet unexplained. However, at $x = 0.5$, 10% of free Cr_2O_3 or of $(Cr_xV_{1-x})_2O_3$ with $x > 0.90$ would be necessary to produce the observed change in neutron reflection intensity. The electron spin resonance results showed that not more than 0.02% of free Cr_2O_3 was present, and microprobe analysis showed the $CrVO_3$ sample prepared at 1300°C to be extremely homogeneous. X-Ray powder patterns, both Guinier and diffractometer, showed only a single corundum phase to be present, and we must conclude that this transition is real. The transition could not be observed for $x < 0.4$, and may shade off to short-range order as x decreases in the same way as the hematite order in the Fe_2O_3–V_2O_3 system (*36*).

4.2. Magnetic Ordering

The Néel temperature curve which defines the lower-temperature AFM phase of Cr_2O_3 type passes through zero at $x = 0.3$ rather than 0.2 as indicated by the rather broad magnetic-susceptibility inflections (*8*), and it is striking that the same curve is also followed in the Cr_2O_3–Al_2O_3 system (*12*) and that the $CrTiO_3$ value also falls on it. With this similarity in mind we have plotted the normalized Néel temperatures (T_N at composition x divided by T_N at $x = 1$) for magnetic ordering in

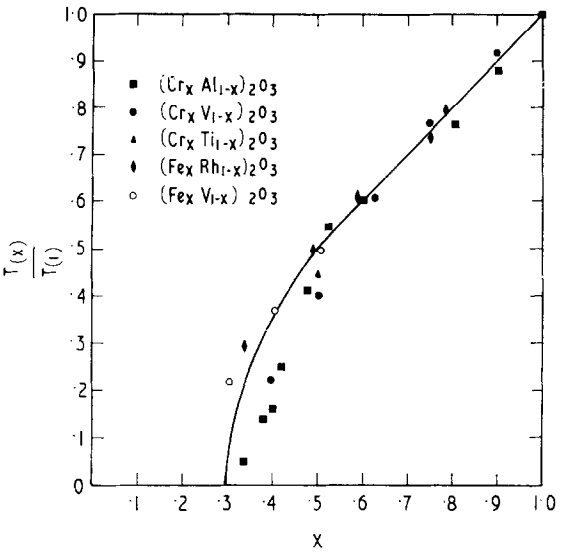

FIG. 7. Normalized Néel points vs composition in corundum type compounds. $(Cr_xAl_{1-x})_2O_3$ Ref. (*11*), $(Cr_xV_{1-x})_2O_3$ this work, $CrTiO_3$ this work, $(Fe_xV_{1-x})_2O_3$ Ref. (*34*), $(Fe_xRh_{1-x})_2O_3$ Ref. (*33*).

these and the Fe_2O_3–Rh_2O_3 (*37*) and Fe_2O_3–V_2O_3 (*36*) systems, Fig. 7. In all cases the $T(x)/T(1)$ values vs composition fall together. Thus substitutions of Al^{3+}, Ti^{3+} or V^{3+} in the Cr_2O_3 lattice act primarily to dilute the magnetic Cr–Cr interactions so that a lower temperature is required for spin ordering. Rh^{3+} (*37*) and V^{3+} (*36*) have a similar effect on Fe_2O_3 type ordering, and Cox, Takei, Miller and Shirane (*36*) concluded that their neutron diffraction data for the Fe_2O_3–V_2O_3 system could be interpreted satisfactorily on the basis of a model involving interactions between Fe^{3+} ions as in Fe_2O_3 without participation from the V^{3+} ions. The behaviour of all these systems is explicable in terms of percolation theory, as discussed in a subsequent paper. A similar effect will presumably be obtained with any other diamagnetic or paramagnetic ion which does not have orbital symmetry appropriate to overlap with Cr^{3+} or Fe^{3+}.

A comparable situation occurs in the $(Cr_xV_{1-x})_2O_3$ monoclinic-hexagonal transformation for $0 < x \leqslant 0.4$. Here the V_2O_3 spin ordering, ferromagnetic in planes corresponding to (110) of the hexagonal structure, and therefore perpendicular to the hexagonal (001) planes in which Cr^{3+} spins are ferromagnetically aligned, proceeds independently of the Cr^{3+} additions apart from a dilution effect. It could be presumed that other diamagnetic or paramagnetic ions would give the same monoclinic → hexagonal temperature–composition boundary.

However, although Cr_2O_3-type spin ordering is dominant at low temperature for $(Cr_xV_{1-x})_2O_3$, $0.4 < x < 0.5$, in the monoclinic region competition between the mutually perpendicular spin systems of V_2O_3 and Cr_2O_3 type leads to complex short-range order. Short-range order was also observed for 70% of V_2O_3 in Fe_2O_3 (*36*). An even more pronounced effect is observed in the middle region of the Cr_2O_3–Fe_2O_3 system, where neither of these strongly spin-ordered structures dominates but instead, despite randomization of Fe and Cr, complex spiral spin order results (*27*).

Acknowledgments

We are indebted to Mrs. C. Li for skilful preparation of most of the samples used in this investigation and to Dr. P. M. Kelly for microprobe analysis.

Note added in proof: P. V. Geld *et al.* (*38*) have also reported on Cr_2O_3–Ti_2O_3 compositions. Unlike them, we observed for $CrTiO_3$ only one inflection, at 135°K, in the variation of the $(012)_{Hexagonal}$ reflection intensity with temperature. In addition, the magnetic susceptibility of our $CrTiO_3$ sample, which contained less than 40 ppm of Fe, showed no field dependence.

References

1. H. Shaked and S. Shtrikman, *Solid State Commun.* **6**, 425 (1968).
2. E. P. Warekois, *J. Appl. Phys.* **31**, 346S (1963).
3. D. Adler, *Solid State Phys.* **21**, 1 (1968).
4. A. Paoletti and S. J. Pickart, *J. Chem. Phys.* **32**, 308 (1960).
5. H. Kendrick, A. Arrott, and S. A. Werner, *J. Appl. Phys.* **39**, 585 (1968).
6. R. M. Moon, *Phys. Rev. Lett.* **25**, 527 (1970).
7. R. M. Moon, T. Riste, and W. C. Koehler, *Phys. Rev.* **181**, 920 (1969).
8. A. Menth and J. P. Remeika, *Phys. Rev.* **B2**, 3751 (1970).
9. B. C. Frazer and P. J. Brown, *Phys. Rev.* **125**, 1283 (1962).
10. P. R. Elliston, *Can. J. Phys.* **47**, 1865 (1969).
11. M. Rubinstein, *Phys. Rev.* **B2**, 4731 (1970).
12. T. M. Sabine and E. R. Vance, *J. Solid State Chem.* **1**, 554 (1970).
13. C. T. Prewitt, R. D. Shannon, D. B. Rogers, and A. W. Sleight, *Inorg. Chem.* **8**, 1985 (1969).
14. R. E. Newnham and V. M. de Haan, *Z. Krist.* **117**, 235 (1962).
15. P. D. Dernier, *J. Phys. Chem. Solids* **31**, 2569 (1970).
16. D. B. McWhan and J. P. Remeika, *Phys. Rev.* **B2**, 3734 (1970).
17. R. D. Shannon and C. T. Prewitt, *Acta Cryst.* **B25**, 925 (1969).
18. A. Jayaraman, D. B. McWahn, J. P. Remeika, and P. D. Dernier, *Phys. Rev.* **B2**, 3751 (1970).
19. A. F. Reid and T. M. Sabine, *J. Solid State Chem.* **2**, 203 (1970).
20. M. Foex and C. Martinez, *Bull. Soc. Chim. Fr.* **17**, 1301 (1950).
21. J. Jaffray and R. Lyland, *J. Rech. Cent. Nat. Rech. Sci.* **4**, 249 (1952).
22. P. D. Dernier and M. Marezio, *Phys. Rev.* **B2**, 3771 (1970).
23. C. T. Anderson, *J. Amer. Chem. Soc.* **58**, 546 (1936).
24. T. R. McGuire, E. J. Scott, and F. H. Grannis, *Phys. Rev.* **102**, 1000 (1956).
25. C. P. Poole and J. F. Itzel, *J. Chem. Phys.* **41**, 287 (1964).
26. D. E. Cox, W. J. Takei, and S. Shirane, *J. Phys. Chem. Solids* **24**, 405 (1963).
27. A. F. Reid and M. J. Sienko, *Inorg. Chem.* **6**, 521 (1967).
28. J. B. Goodenough, "Magnetism and the Chemical Bond," John Wiley and Sons, New York, 1963.
29. W. Rudorff and B. Reuter, *Z. Anorg. Chem.* **253**, 177 (1947).
30. R. Plumier and A. Tardieu, *C. R. Acad. Sci. Paris* **257**, 3858 (1963).
31. J. M. Hastings, L. M. Corliss, W. Kunnmann, and S. La Placa, *J. Phys. Chem. Solids* **28**, 1089 (1967).
32. R. Norrestam, *Arkiv Kemi* **29**, 343 (1968).
33. O. Halpern and M. H. Johnson, *Phys. Rev.* **55**, 898 (1939).
34. L. M. Corliss, J. M. Hastings, R. Nathans, and G. Shirane, *J. Appl. Phys.* **36**, (2) (1965).
35. F. J. Morin, *Phys. Rev. Lett.* **3**, 34 (1959).
36. D. E. Cox, W. J. Takei, R. C. Miller, and G. Shirane, *J. Phys. Chem. Solids* **23**, 863 (1962).
37. E. Kren, P. Szabo, and G. Konczos, *Phys. Lett.* **19**, 103 (1965).
38. P. V. Geld, V. G. Zubkov, and I. I. Matveenko, *Phys Status Solidi.* (b) **46**, 187 (1971).